ISTITUTO NAZIONALE DI FISICA NUCLEARE

Sezione di Milano

INFN/TC-00/07
17 Maggio 2000

A MODEL OF THE CURRENT DISTRIBUTION INSIDE THE RESISTIVE JOINTS OF THE ATLAS TOROIDS

Giovanni Volpini

INFN-Sezione di Milano, Laboratorio LASA, via f.lli Cervi 201, 20090 Segrate (MI), Italy

Abstract

The eddy currents generated inside a cable joint may have remarkable consequences both during measurements on test joints and also during magnet operation. In the latter case the induced currents may be very high, possibly exceeding the critical value. Also the power dissipated by the resistive decay of such currents can be many times larger than the steady state value. These eddy currents -and therefore the dissipation- can be significantly reduced by means of a suitable choice of the joint length.

PACS: 85.25.L

Published by ***SIS–Pubblicazioni***
Laboratori Nazionali di Frascati

CONTENTS

1 INTRODUCTION

Several resistive joints are foreseen inside ATLAS Barrel Toroids, between the two pancakes of each section of the coil, between the two sections of each coil and between different coils. The problems due to the Joule heating under stationary conditions have been already described [1]. Here we address ourselves to the non-stationary effects: during the magnet charge the magnetic field component normal to the joint induces large currents that may have remarkable consequences, since they increase the Joule dissipation, and possibly exceed the critical current value. Non-stationary effects are also relevant during test joints measurements; due to the inductance of the joint, the current is not distributed evenly along the joint, and this distribution changes over the time. This effect must be kept into account during the data analysis.

In this note:

i) we present a simple model of the joint, based on a resistors - inductances network;

ii) we show that this model explains fairly well the experimental results on a test joint. This allows us to obtain experimental estimates of the model free parameters. We skip the experimental details, described elsewhere [2].

iii) We apply the model to the coil joints assuming the appropriate geometry of this situation and the experimental values for the free parameters. We make estimates of the current profile during the magnet ramp and dump (exponential) discharge. We analyse the consequences from the thermal and electrical point of view.

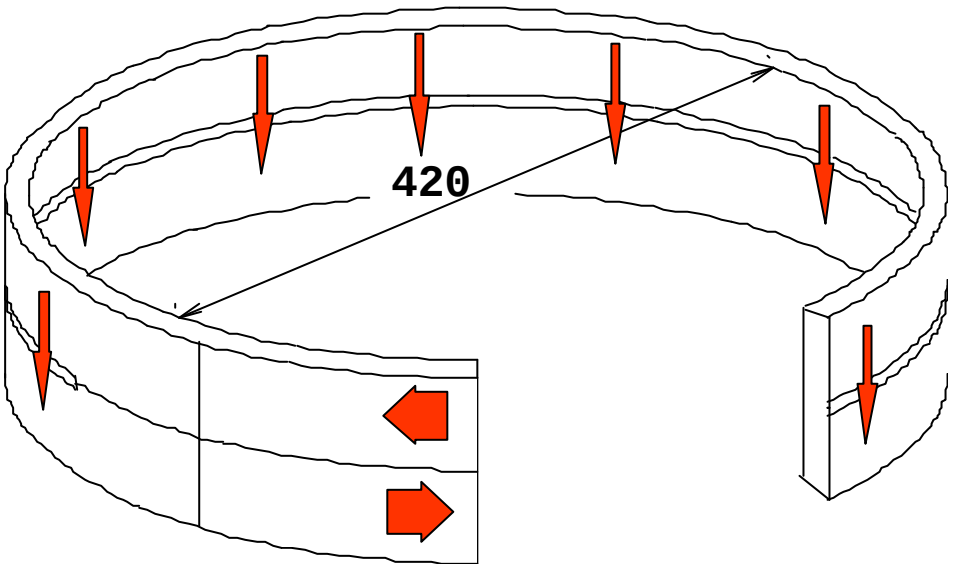

FIG. 1: Sample layout composed of two conductors welded along the narrow faces. The arrows describe the current flow. This sample was used for specific resistance measurements.

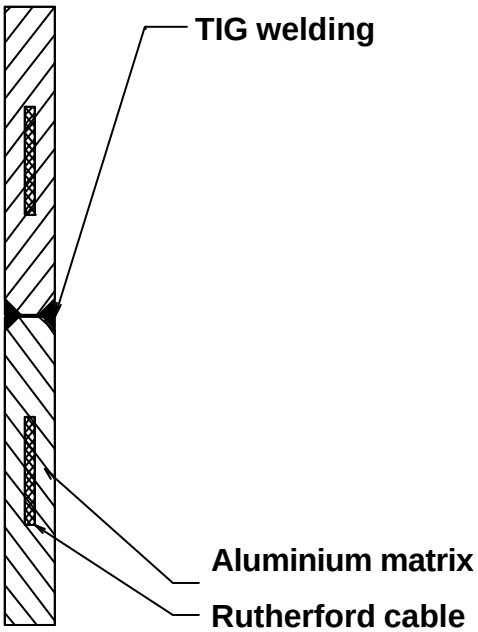

FIG. 2: Cross section of the joint shown in Fig. 1. The layer-to-layer joint inside a pancake presents the same geometry.

2 THE MODEL

The model is based on a joint between two Aluminium-stabilised superconducting cables, welded along their narrow faces (see Fig. 1 and 2). The joint length is L. The resistive path between the two Rutherford's may be described as a set of N resistors with resistance R, while the inductive effects due to the closed loop circuit is described by the $2(N-1)$ inductors with inductance L and mutual inductance between the corresponding inductors of the two layers M (see Fig.'s 3 and 4).

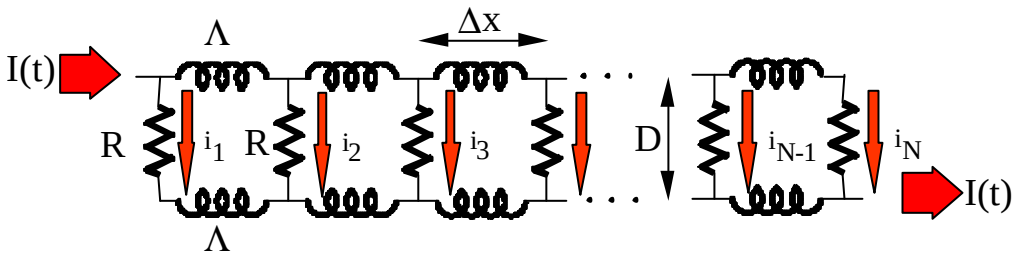

FIG. 3: Lump elements model of a layer-to-layer joint. As explained in the text, all resistors and inductors are equal, with values R and L, and mutual inductance M.

We assume the joint to be homogenous so that all the resistors and inductors are similar, we neglect furthermore the end effects (the current flow takes place normally with respect to the Rutherford) as well as the mutual coupling between loops. This last assumption is reasonable

since the lines of the magnetic self-field lie mainly in planes orthogonal with respect to the conductor axis. The scheme depicted in Fig. 3 is appropriate for a joint inside the coils, while for a test joint the current enters in the upper conductor from one side and exits from the lower conductor on the same side (Fig. 4).

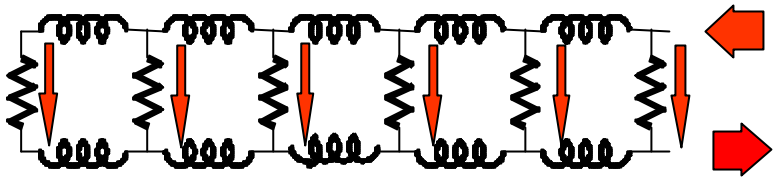

FIG. 4: Lump elements model of the test joint shown in Fig. 1 . The main features are the same as in Fig. 3, only the current enters and exits from the same side.

The current flow in all the loops is described by a set of *N-1* equations. We shall see later that we can pass from this lump elements model to a model with distributed resistance and inductance. In this case the current flow is described by a parabolic differential equation. This equation may be solved analytically provided that its coefficients are constant. In our case this is not strictly true, since the specific resistance changes during the process because of the magnetoresistance. For this reason we solve the problem also numerically; analytical solutions remain useful both for comparison and to get quick results.

3 THE CURRENT DISTRIBUTION INSIDE A JOINT.

3.1 Test joint.

Our model is composed by *N-1* loops (Fig. 4). For each loop we may write:

$$2\cdot\left(\Lambda - M\right)\cdot\frac{d}{dt}\sum_{n=j}^{N-1} i_{n+1} + R\cdot\left(i_{n+1} - i_n\right) = 0 \qquad j = 1, 2 .. N-1 . \qquad (1)$$

Now if we let *N* tend to infinity and divide (1) by $\Delta x = L/N$ we pass to the continuum:

$$2\cdot\frac{\Lambda - M}{\Delta x}\cdot\frac{d}{dt}\sum_{n=j}^{N-1} i_{n+1} + R\cdot\Delta x\cdot\frac{d}{dx} j = 0 . \qquad (2)$$

Here we have introduced a linear current density *j(x)*. The summation over *n* is then replaced by an integral, so that eventually we get:

$$2\cdot(\lambda-\mu)\cdot\frac{d}{dt}\int_x^L j(u,t)\,du+\rho\cdot\frac{d}{dx}j(x,t)=0 \quad . \tag{3}$$

Introducing the following position,

$$J(x,t)=\int_x^L j(u,t)\,du \quad , \tag{4}$$

(3) may be reduced to the standard diffusion-type (parabolic) differential equation:

$$\frac{d}{dt}J(x,t)-\frac{\rho}{2\cdot(\lambda-\mu)}\cdot\frac{d^2}{dx^2}J(x,t)=0\,. \tag{5}$$

This equation describes the current flow at each point of the joint at any time. It must be completed by boundary conditions, which in our case are:

$$\begin{aligned} J(0,t)&=I(t)\\ J(L,t)&=0 \end{aligned} \quad , \tag{6}$$

where *I(t)* is a known function describing the total current fed into the joint at time *t*.

3.2 Joint inside coils.

In this case (see Fig. 3) the equivalent of (1) is:

$$(\Lambda-M)\cdot\frac{d}{dt}\left(-\sum_{n=1}^{j}i_n+\sum_{n=j+1}^{N}i_n\right)+R\cdot(i_{j+1}-i_j)=-\frac{d}{dt}\Delta\Phi=-D\cdot\Delta x\cdot\frac{d}{dt}B \quad . \tag{7}$$

$$j=1,2..N-1$$

Where *DF* is the flux linked to each loop, which is equal to the mean distance between the two Rutherford cables, *D*, times the small interval *Dx* times the normal component of the magnetic field at the joint, *B*. The reduction to the continuous form is strictly analogous to what we have seen above. In this case we get:

$$(\lambda-\mu)\cdot\frac{d}{dt}\left(-\int_0^x j(u,t)\,du+\int_x^L j(u,t)\,du\right)+\rho\cdot\frac{d}{dx}j(x,t)=-D\cdot\frac{d}{dt}B$$

$$(\lambda-\mu)\cdot\frac{d}{dt}\left[-\left(\int_0^L j(u,t)\,du-\int_x^L j(u,t)\,du\right)+J(x)\right]+\rho\cdot\frac{d}{dx}j(x,t)=-D\cdot\frac{d}{dt}B\,. \qquad (8)$$

$$\frac{d}{dt}(2\cdot J(x,t)-J(0,t))-\frac{\rho}{\lambda-\mu}\cdot\frac{d^2}{dx^2}J(x,t)=\frac{-D}{\lambda-\mu}\cdot\frac{d}{dt}B$$

The boundary conditions are the same as above, (6), so that we can eventually write:

$$\frac{d}{dt}J(x,t)-\frac{\rho}{2\cdot(\lambda-\mu)}\cdot\frac{d^2}{dx^2}J(x,t)=\frac{d}{dt}\left[\frac{-D}{2\cdot(\lambda-\mu)}\cdot B+\frac{I(t)}{2}\right]=\beta\cdot\frac{dI}{dt}\,, \qquad (9)$$

where $\beta=\frac{I(t)}{2}-\frac{D\cdot k}{2\cdot(\lambda-\mu)}$ and $k=\frac{B_r}{I_{max}}$.

The two cases a) and b) are therefore described by analogous equations, (5,6), for case a) and (9,6) for case b), the difference being given by the presence of a source term in the latter case, due to the linked flux. These equations may be solved analytically provided that the coefficients are constant. In our case $l-m$ depends only on the geometry and may be assumed as constant; on the other hand r depends on the magnetoresistance and therefore on the total current flowing in the BT. In the case of a test joint we still can assume r as constant since the contribution of the self field is negligible as compared to the applied external field. We conclude that the analytical solution is fully satisfactory in the case of a test joint, while for a real joint inside the coils we must solve numerically (9,6). We shall see later that the numerical results do not differ significantly from the analytical ones, which give also a better insight on the role played by the different parameters. Analytical and numerical solutions are also useful since they validate each other. The detailed derivation of analytical solutions is given in the Appendix.

4 TEST JOINT: MEASUREMENTS RESULTS

4.1 The solution

In this case we assume (as we have done in the measurements) that the current goes from zero to a fixed value with constant ramp rate, then it remains at that value for some time, and finally it comes back to zero with the same ramp rate (see Fig. 5, where we have reported the actual values used in the joint resistance measurement shown in Fig. 8).

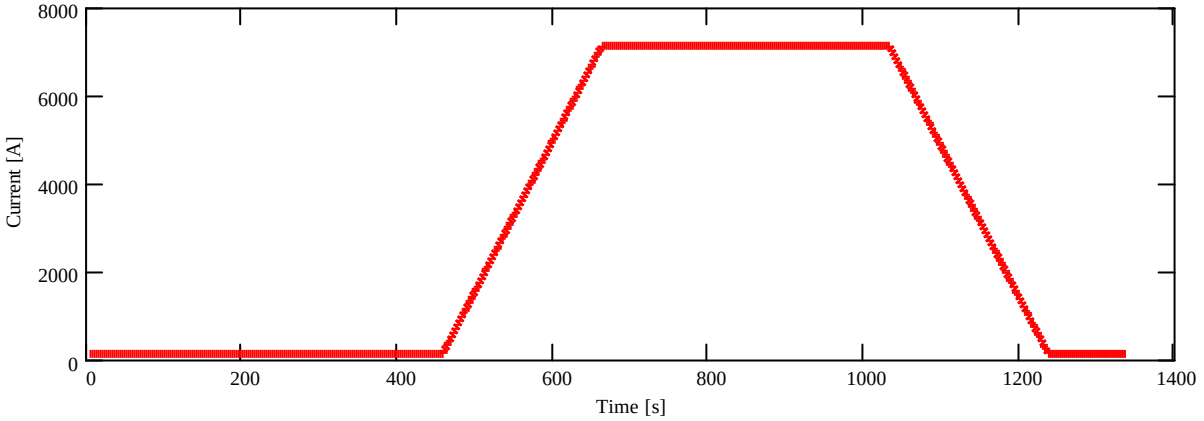

FIG. 5: The current ramp exploited in the measurement of the joint resistance.

The solution of this problem is described in Appendix A.2. Here we report only the final result for the current density:

$$j(x,t) = \frac{1}{L}\cdot\left(I(t) - \pi\cdot \sum_{n=1}^{\infty} Y_n(t)\cdot n\cdot \cos\left(n\cdot\pi\cdot\frac{x}{L}\right)\right), \qquad \text{(A.29)}$$

where $Y_n(t)$ are the functions:

$$Y_n(t) = \frac{-2\cdot I_{dot}\cdot\alpha}{(n\cdot\pi\cdot\alpha)^3}\cdot\left[e^{(n\cdot\pi\cdot\alpha)^2\cdot MN0(t_3,t)} - e^{(n\cdot\pi\cdot\alpha)^2\cdot MN0(t_2,t)} \ldots \right.$$
$$\left. + e^{(n\cdot\pi\cdot\alpha)^2\cdot MN0(t_4,t)} - e^{(n\cdot\pi\cdot\alpha)^2\cdot MN0(t_5,t)} \right] \qquad \text{(A.27)}$$

where: $MN0(x,y)=\Phi(y-x)\cdot(x-y)$, Φ is the Heaviside step function, and

$$\alpha = \sqrt{\frac{\rho}{2\cdot(\lambda-\mu)\cdot L^2}}\ . \qquad \text{(A.5a)}$$

Equation (A.29) gives the current density distribution at any point of the joint at any time. This equation contains the following parameters: L (joint length), I_{dot} (current ramp rate), r and l-m (through a). The first two are known from experimental conditions, while the last two may be deduced from the measurements.

4.2 Discussion of the solution

To understand better the solution behaviour, let us first focus to its time dependence. We therefore select quite arbitrarily four locations along the joint, at x/L = 0, 0.25, 0.5, 0.75 (that is, at the beginning, at one fourth of its length, midway and at three fourths), and we see how the current density evolves with time at these places (Fig. 6).

In Fig. 7 we revert the approach, and we investigate the current density profile along the whole joint at some given times, specified in the caption.

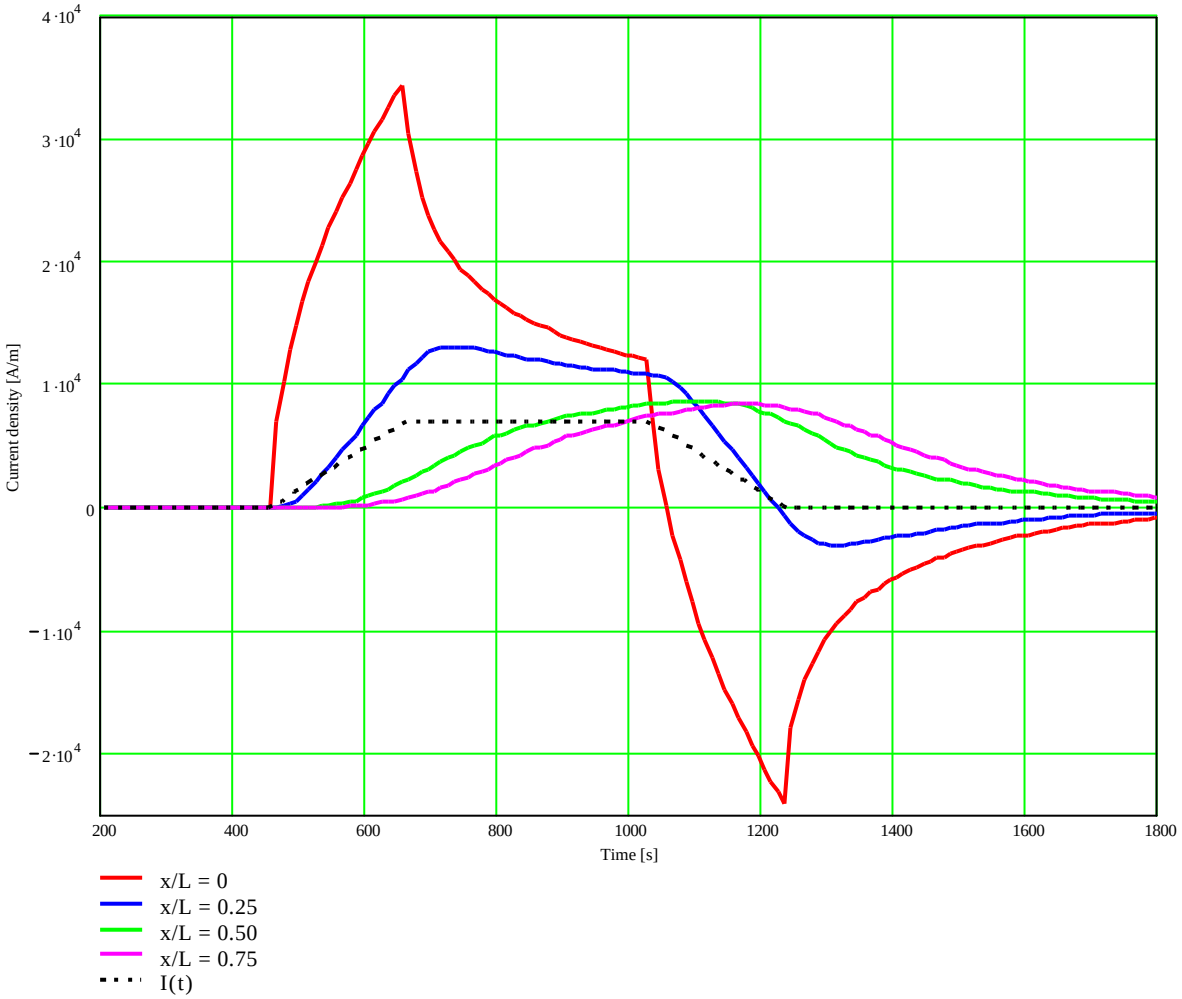

FIG. 6: Current density as a function of time at four locations along the joint. The dash line represents the external current (in amperes) flowing into the sample, also shown in Fig. 5.

As it can be seen, the current rises faster near the beginning of the joint, and at the end of the ramp is still unevenly distributed; later it relaxes approaching an even profile which is never reached because the external current begins to decrease; also when the external current is zero the Foucault currents (whose slower component decays with time constant $(\pi\cdot\alpha)^{-2}$) still flow inside the joint.

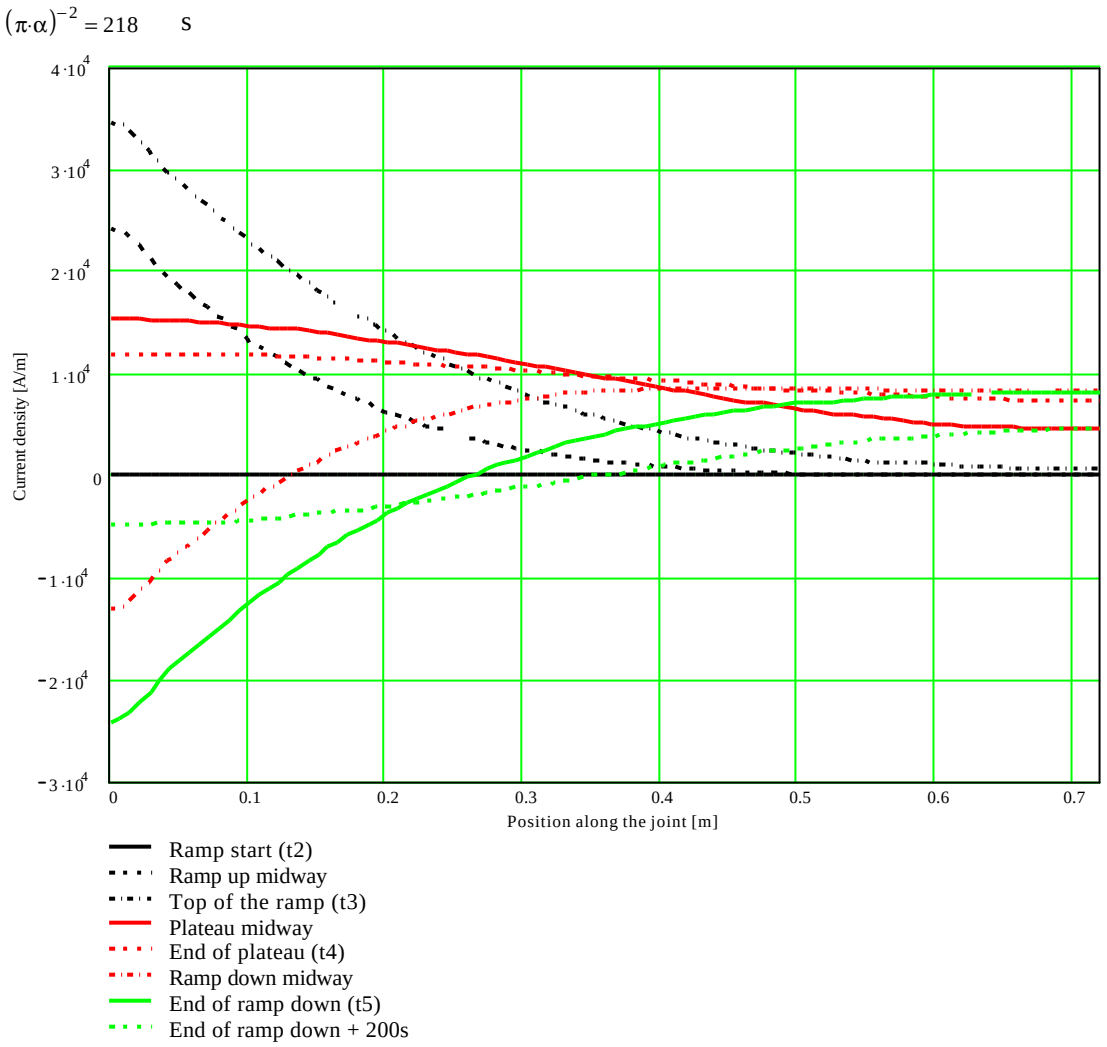

FIG. 7: Current density profiles along the joint, 0.721 m long, at some given instants. The corresponding current *I(t)* is shown in Fig. 5.

4.3 Experimental Investigation and Conclusions

The model described here above has been developed in order to explain the measurements whose primary goal was to measure the specific resistance *(r/L)* of a joint. We have performed a best fit procedure applying (A.29), (times r) to our measurements of voltage drop at some known locations along the joint, leaving r and $l-m$ as free parameters. The quality of the fit may be appreciated from Fig. 8. The values of r and $l-m$ used, which therefore represent the experimental estimates, are:

$$\begin{aligned} r &= 1.45\cdot10^{-10}\ \Omega\cdot\text{m} \\ l-m &= 3\cdot10^{-7}\ \text{H/m} \end{aligned} \quad . \tag{10}$$

All the details of the experimental procedure are described in [2]. Measurements shown in Fig. 8 were performed with no applied magnetic field. Measurements with applied magnetic field up to 4 T have been done also. Although the experimental data were much

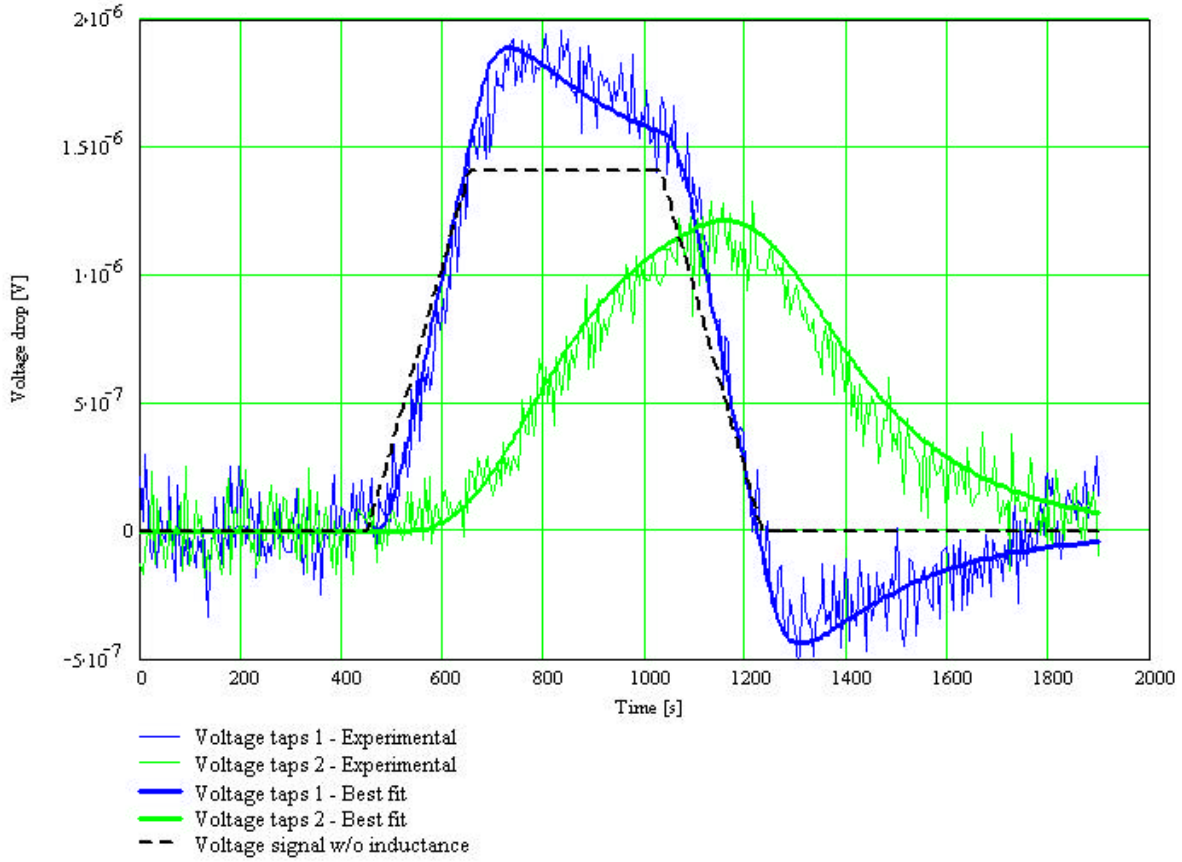

FIG. 8: Results from a measurement of the voltage drop along a joint at two different positions, superimposed with the curves from a best fit procedure.

more noisy, it was possible to measure the specific resistances at all fields, even if with larger uncertainties.

We can summarise the most important conclusions from these measurements as follows:

i) the model introduced in Sec. 2 describes very well the experimental data with only two free parameters. It seems therefore sound to use the same model to predict the behaviour of the current distribution in a joint inside the magnet; and

ii) we have experimental values for $r(B)$ and $l-m$ at disposal.

5 JOINTS INSIDE COILS: BEHAVIOUR DURING NON-STATIONARY CONDITIONS

We now want to investigate the current distribution inside a joint, keeping into account the coupling with the radial magnetic field. In particular we want to determine the amount of Foucault currents in order to see if these can exceed the critical value or introduce a significant increase of the Joule dissipation. Here we exploit the model described by (9,6). We analyse three operating conditions; i) the magnet charge with constant ramp rate, followed by a long plateau at the operating current, ii) the discharge with constant ramp rate, after a long-lasting period at constant current (Sec. 5.1), and iii) the discharge with exponential current decay (dump discharge) in Sec. 5.2.

5.1 Magnet charge and discharge with constant ramp rate.

5.1.1 The analytical vs. numerical approach

The analytical solution for current density profile is determined in Appendix A.3. The same solution applies both to the charge and to the discharge, provided that I_{dot} has the right sign and the correct *I(t)* is exploited. The general form of the solution is identical to the previous case:

$$j(x,t) = \frac{1}{L}\cdot\left(I(t) - \pi\cdot \sum_{n=1}^{\infty} Y_n(t)\cdot n\cdot \cos\left(n\cdot\pi\cdot\frac{x}{L}\right)\right). \qquad (A.35)$$

Where the $Y_n(t)$ now are:

$$Y_n(t) = \frac{2\cdot I_{dot}\cdot\alpha}{(n\cdot\pi\cdot\alpha)^3}\cdot\left[\beta\cdot\left[1-(-1)^n\right]-1\right]\cdot\left[\begin{matrix} e^{(n\cdot\pi\cdot\alpha)^2\cdot MN0(t_1,t)} \ldots \\ +\left[-e^{(n\cdot\pi\cdot\alpha)^2\cdot MN0(t_0,t)}\right]\end{matrix}\right], \qquad (A.33)$$

and *MN0(x,y)* is defined as above. In this case we are interested also to the integrated current density, which represents the current flowing inside the upper Rutherford cable:

$$J(x,t) = I(t)\cdot\left(1-\frac{x}{L}\right) + \sum_{n=1}^{\infty} Y_n(t)\cdot\sin\left(n\cdot\pi\cdot\frac{x}{L}\right), \qquad (A.34)$$

where the functions $Y_n(t)$ are again as (A.33). The current flowing along the lower Rutherford at x is simply given by the external current, *I(t)*, minus the current in the upper Rutherford at the same position x. The current profiles are not symmetrical since the Foucault current flow may take place clockwise or anticlockwise depending on the sign of the radial component of the magnetic field (the sign of k). In the following analysis we will present only the profile with the highest peak current, since this represents the worst case. As we said before, analytical solutions based on constant coefficients are not fully satisfactory in this case, since due to the magnetoresistance the joint specific resistance changes of a factor 3-4 passing from 0 to 4 T. We have developed a finite-differences program to solve the parabolic differential equation with non-constant coefficients. This program is written in FORTRAN and it adopts an explicit method to compute the next time step.

5.1.2 Current flowing inside the Rutherford cable

We report below the current distributions inside the Rutherford calculated numerically (symbols) assuming the expression for $r(B)$ shown in Fig. 9; for both the ramp up (Fig. 10) and ramp down (Fig. 11). In the same graphs we have plotted for reference the results computed from the analytical solutions assuming proper constant values for r, as explained in the captions. The main parameters exploited in the simulations are listed in Table 1.

TAB. 1: Parameters used in the simulations.

	Symbol	Value
Average distance between the two Rutherfords	D	0.057 m
Normal (radial) magnetic field at the joint [1]	B_r	0.77 T
Operating current	I_{max}	20.5 kA
Field/current ratio	$k = B_r / I_{max}$	$3.756\ 10^{-5}$ T/A
ATLAS Toroids ramp rate	I_{dot}	2.847 A/s
Joint length	L	Variable

A critical point is the value of the specific resistance that changes largely in presence of an applied magnetic field. Keeping into account both the results of the measurements described in this note and of subsequent measurements [3], we have an acceptable experimental description of the joint magnetoresistance between 0 and 4 T (see Fig. 9). We

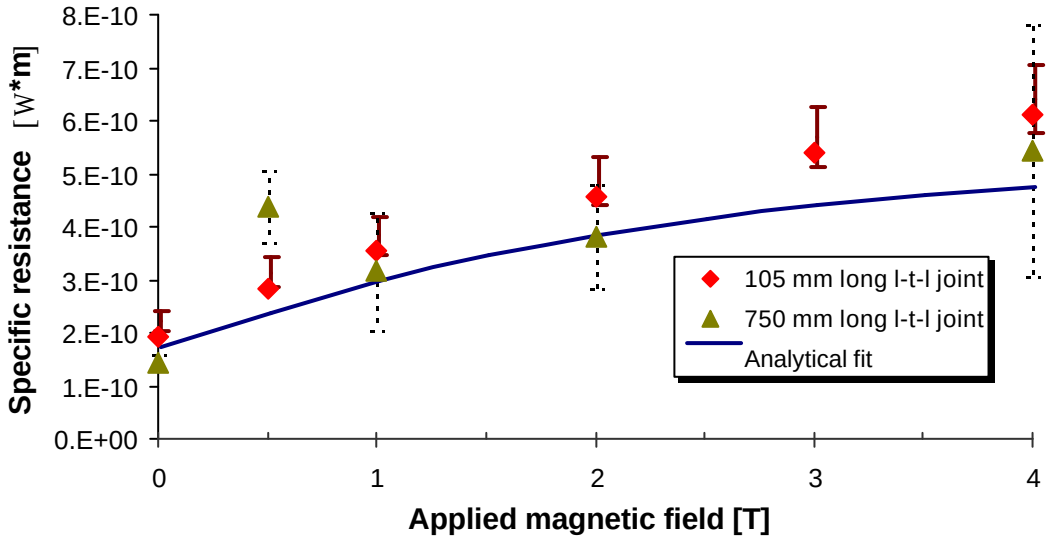

FIG. 9: Joint magnetoresistance. Triangles are from the experimental results described in this note, square are the results appeared in [3]. The analytical fit is described in the text.

[1] Note that the sign reverses from one double pancake to the other.

have therefore chosen a possible interpolation function of the form $\rho(B) = \rho_0 \cdot \left(1 + a \cdot \mathrm{atan}\left(B \cdot b^{-1}\right)\right)$. This expression depends on the zero-field specific resistance (r_0) times a term in brackets that describes the magnetoresistance. While the former term depends on the sample geometry, the latter should not. At the same time the experimental uncertainties on the zero-field specific resistances are comparable while the in-field results are much more accurate on the shorter sample. Since the most conservative assumption is made with lowest resistance, which yields the highest eddy currents, we have chosen i) the zero-field value ($r_0 = 1.45 \cdot 10^{-10}$ Ωm) from the longer sample, and ii) the magnetoresistance contribution (a=1.928, b=2.139) from the shorter sample, which has the lower experimental uncertainty (Fig. 9).

Magnet Ramp-up

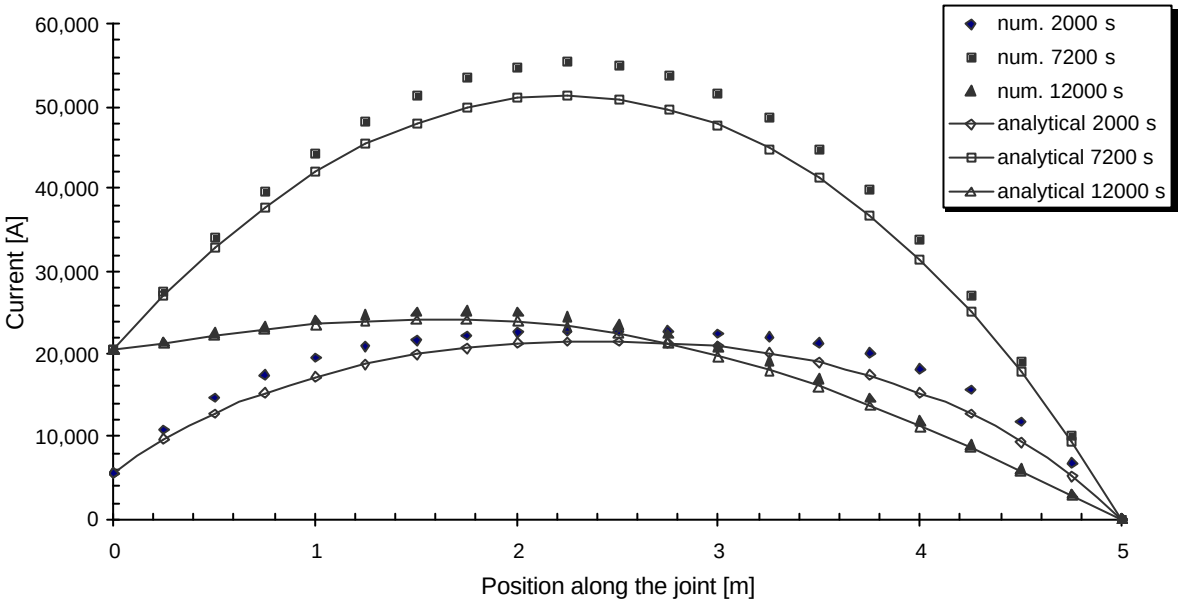

FIG. 10: Current distribution along the joint during the magnet charge. The points (lines) are the numerical (analytical) results. The specific resistance value adopted in the analytical curves is $3.93 \cdot 10^{-10}$ Ωm, corresponding to 2.62 T, that is the value reached in the joint when the Toroid magnetic field is at its maximum. As it can be seen, the difference between the two approaches is small. The analytical method underestimates the peak current since it assumes the final (highest) value for r, while in the numerical computations r grows with the external current reaching that value only at the end of the current ramp.

Magnet Discharge

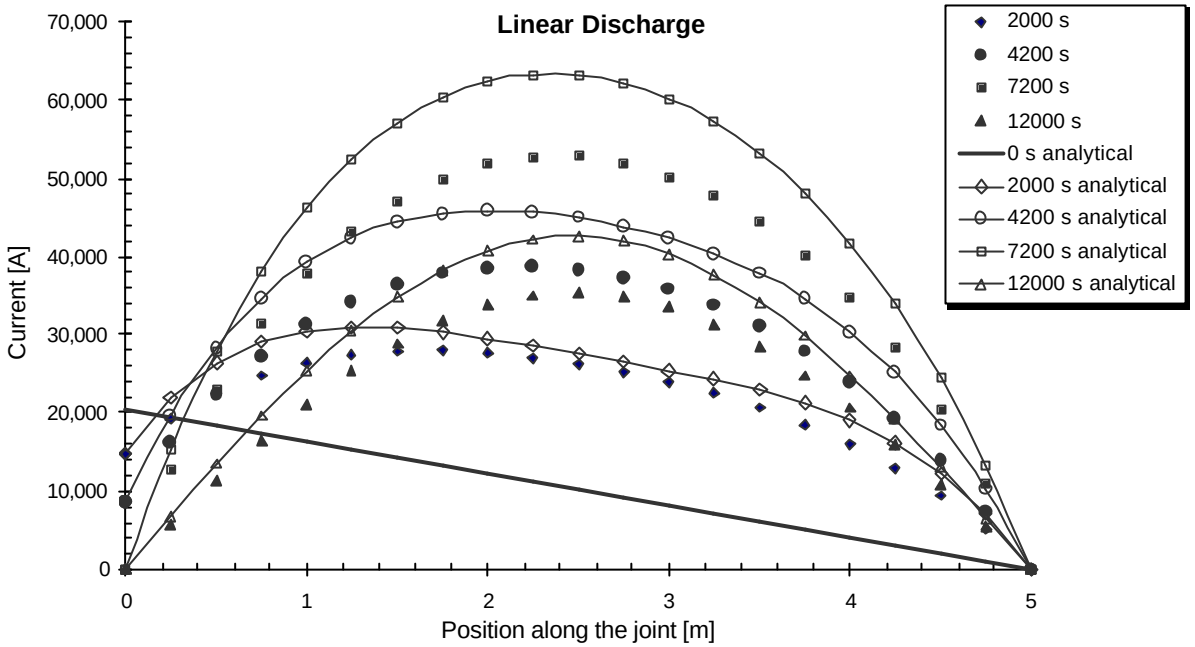

FIG. 11: Current distribution along the joint during the magnet discharge. The points (lines) are the numerical (analytical) results. The specific resistance value adopted in the analytical curves is $1.45 \cdot 10^{-10}$ Ωm, corresponding to 2.62 T, that is the value reached in the joint when $I = 20.500$ A. Here the agreement is much worse than it was in Fig. 10. This can be understood as follows: the joint magnetoresistance grows largely with the magnetic field. As a consequence, during the ramp-up the highest resistance value is almost immediately attained, and then it remains constant, so that we do not make a large error assuming its value as constant since the beginning. On the other hand, during the magnet discharge the specific resistance changes significantly during the process, since it remains close to its higher value as long as the current is nonzero (and in fact at t=2000 s the agreement is still good), and then it attains the (much lower) value at B=0.

We can conclude that during the magnet charge the analytical (with constant r) and numerical approaches give results in agreement within 10% or less. This is not true during the discharge, and in this case we must rely mainly on numerical computations. We note briefly that we made -as a check- numerical computations with constant r. Results were identical to the analytical ones. In Fig. 14 we report the highest current, calculated numerically, in the Rutherford during the magnet charge and discharge with a constant ramp rate.

5.1.3 Scaling laws for the peak current

In this section we determine an expression for the peak current during the magnet charge. The peak current is reached at the end of the current ramp-up, at about one half of the joint length, as it can be seen in the above figures. Its value is therefore found from (A.34), estimated at $x=L/2$, $t=t_1$:

$$J_{peak} = \frac{I_{max}}{2} - \frac{2 \cdot I_{dot} \cdot D \cdot k}{\alpha^2 \cdot \pi^3 \cdot \lambda} \cdot \sum_{n=0}^{\infty} \frac{(-1)^n}{(2 \cdot n + 1)^3} \cdot \left[1 - e^{[(2 \cdot n+1) \cdot \pi \cdot \alpha]^2 \cdot (t_0 - t_1)} \right]. \quad \text{(A37)}$$

This sum has alternating signs, so that the maximum error is equal to the modulus of the first neglected term; in practice the contribution from the second term (included) on is less than 2%, if the ramp up time is not much smaller than the time constant $(\pi \cdot \alpha)^{-2}$. In this approximation we can write:

$$J_{peak} = \frac{I_{max}}{2} + \frac{4 \cdot I_{dot} \cdot D \cdot k \cdot L^2}{\rho \cdot \pi^3} \cdot \left[1 - e^{(\pi \cdot \alpha)^2 \cdot (t_0 - t_1)} \right]. \quad \text{(A.38)}$$

Assuming the above values and in particular $r = 3.93 \cdot 10^{-10}$ Ωm and $L = 5$m we get a value of 52.5 kA for J_{peak}, to be compared with 55.3 kA from the numerical results. This estimate is therefore quite accurate; nonetheless, (A.38) was determined under specific assumptions (and notably assuming that the highest current takes place near the centre of the joint. This is true only if the induced current is large, otherwise (A.38) fails. This should not be a problem, since the formula is useful when high eddy currents are being considered, and in any case a full numerical computation is advisable. Eq. (A.38) gives also the scaling laws of the peak current. As it can be seen the peak current is the sum of a steady-state term $I_{max}/2$ plus a transient term that scales as $\left(I_{dot} D k L^2\right)/r$; it is worth mentioning that it does not depend on λ. This means that reducing from 5 to 3 m the joint length the peak current should be about 2.5 times lower (see A.5).

5.1.4 Heating due to the induced currents

A further problem for the magnet operation comes from the extra heating due to the induced currents. The total power dissipated along the junction is:

$$Q(t) = \rho \cdot \int_0^L j(x,t)^2 \, dx. \quad \text{(A.39)}$$

Now let us substitute the explicit expression for $j(x,t)$ (A.35), we have:

$$Q(t) = \frac{\rho}{L} \cdot \int_0^1 \left(I(t) - \pi \cdot \sum_{n=1}^{\infty} Y(n,t) \cdot n \cdot \cos\left(n \cdot \pi \cdot s\right) \right)^2 ds. \qquad (A.40)$$

This integral is evaluated in Appendix B. The result shows a very interesting aspect:

$$Q(t) = \frac{\rho \cdot I(t)^2}{L} + \frac{\rho \cdot \pi^2}{2 \cdot L} \cdot \sum_{n=1}^{\infty} Y_n(t)^2 \cdot n^2, \qquad (A.41)$$

that is, the power dissipation is due to two terms: the first represents the joule dissipation due to the transport current (let us call it the 'Joule term'), while the second is related to the induced currents (let it be the 'Foucault term'). In Fig. 12 we investigate how these terms change over the time, assuming a constant specific resistance of $3.93 \cdot 10^{-10}\ \Omega \cdot m$. The Foucault term is maximum at the end of the current ramp, reaching 0.872 W (from numerical computations), to be compared with a steady state value of 0.033 W. The contribution from the Foucault term may be overwhelming during transient conditions. To understand better how the two terms are affected by the different parameters, let us study their scaling behaviour. The Joule term is clear: the power scales as r and as L^{-1} . The ramp rate I_{dot} has obviously no effect. As for the Foucault term, with some algebra (details in Appendix A.5) and introducing the form of a we may cast the Foucault term in the following form, that makes explicit the dependencies on the parameters:

$$\frac{8 \cdot \pi^2 \cdot I_{dot}^2 \cdot \lambda^2 \cdot L^3}{\rho} \cdot \sum_{n=1}^{\infty} y(n,t)^2 \cdot n^2, \qquad (A.42)$$

where the y(n,t) are defined as in (A.31). This tells us that the Foucault term scales as r^{-1}, I_{dot}^2 and as L^3. These dependencies are by far different from the Joule term; a change of a factor 2 for the joint length changes the ratio between the two terms of a factor 16! Specific resistance and ramp rate affect quadratically the ratio. From the numerical computations we discover that if the joint length is reduced to 2.5 m instead of 5 m, the maximum power dissipated by the Foucault currents is 0.205 W, to be compared with a steady state value of 0.066 W. A last issue to be clarified is the consequence on the magnetic field stability of the current redistribution in the joints.

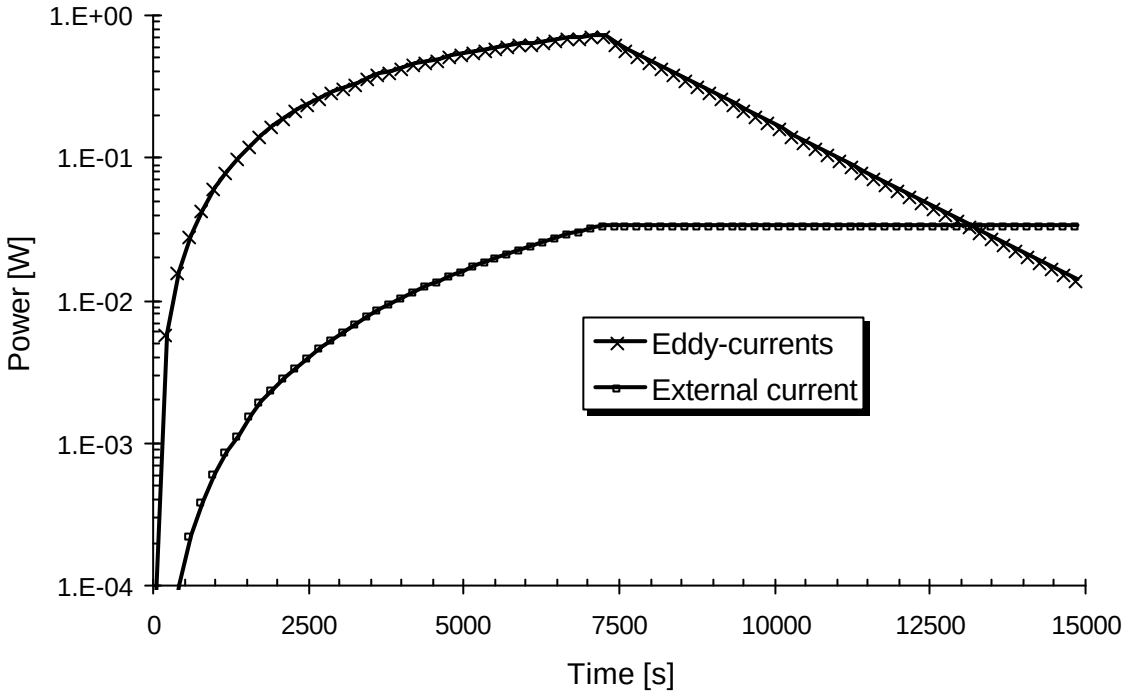

Fig. 12. Power dissipated in a joint 5 m long during the magnet charge, assuming a constant specific resistance of $3.93 \cdot 10^{-10}$ Ωm. The two terms composing (A.41) are reported separately.

5.2 Magnet discharge with exponential current decay.

The analytical solution for this case is evaluated in Appendix A.6. The solution is given always by (A.28):

$$J(x,t) = I(t)\cdot\left(1 - \frac{x}{L}\right) + \sum_{n=1}^{\infty} Y_n(t)\cdot\sin\left(n\cdot\pi\cdot\frac{x}{L}\right), \qquad \text{(A.28)}$$

with the appropriate expressions for $I(t)$ and $Y_n(t)$, (A.43) and (A.44); the function $MN0(x,y)$ is defined as usual:

$$Y(t)_n = -2\cdot I(t_0)\cdot\frac{\beta\cdot\left[1-(-1)^n\right]-1}{n\cdot\pi\cdot\left[(n\cdot\pi\cdot\alpha)^2\cdot\tau - 1\right]}\cdot\left[e^{\frac{MN0(t_0,t)}{\tau}} - e^{\left[(n\cdot\pi\cdot\alpha)^2\cdot MN0(t_0,t)\right]}\right], \qquad \text{(A.44)}$$

$$I(t) = I(t_0)\cdot e^{\frac{t_0 - t}{\tau}} . \qquad \text{(A.43)}$$

Here we report in Fig. 14 the numerical and analytical results found for an exponential current decay with time constant t = 5.14H / 2 mΩ = 2600 s.

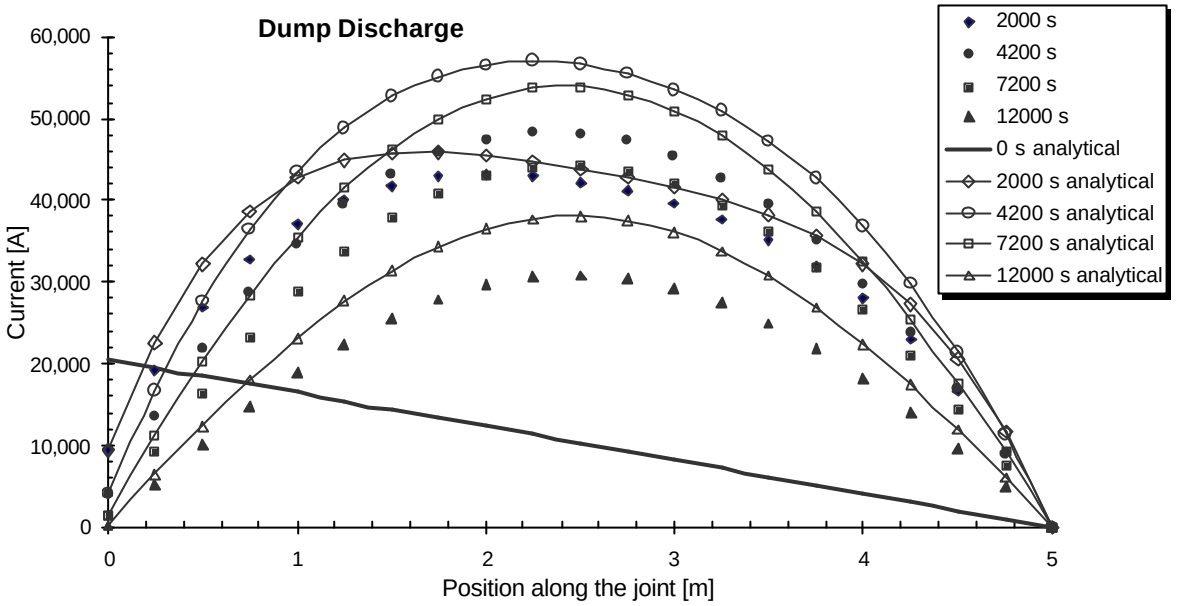

Fig 13. Current distribution along the joint during the magnet dump discharge with t = 2600 s (R_{dump} = 2 mΩ), assuming r = 1.45·10^{-10} Ω·m. The peak current is reached at t = 4200 s. As it can be seen, analytical solutions are accurate only at the beginning of the process, when the specific resistance has not changed very much; an analogous behaviour was observed in Fig. 11. The joint length is 5 m.

Despite the fact that with an exponential decay the initial dI/dt is higher (-7.88 A/s) as compared with the charge ramp-rate (2.85 A/s), the peak current during the dump (exponential) discharge is actually *lower:* this happens because the peak current depends -so to speak- on the integral of the charge/discharge process averaged over thousands of seconds; although the dI/dt of the exponential discharge is higher at the beginning, it gets lower quickly.

5.3 Peak currents and power dissipation as a function of the joint length.

So far we have always assumed a joint length of 5 m. This number was chosen in order to reduce the power dissipation, and therefore the temperature rise, under steady state conditions [1)]. In those calculations we made many conservative assumptions, especially regarding the heat exchange with the surroundings; we assumed that no heat was exchanged with the casing all along the joint length. This assumption could be reasonable

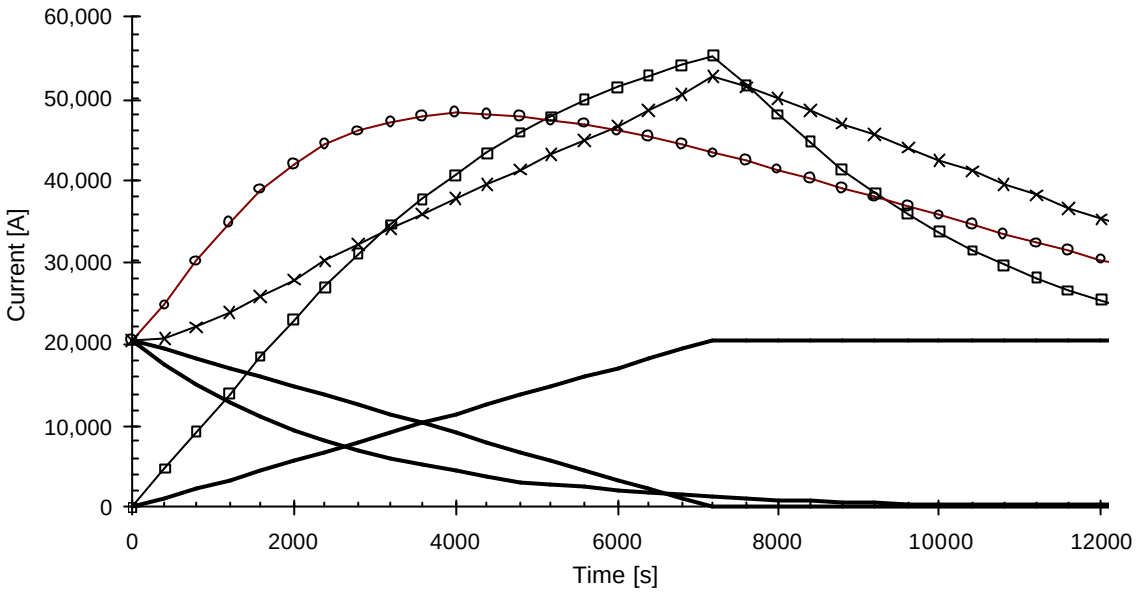

Fig. 14. Highest current in the Rutherford cable during the magnet charge (squares), linear discharge (crosses) and dump (circles) discharge calculated numerically. The external current fed into the magnet is reported also. The joint is assumed to be 5 m long.

for a joint between different coils, but it is doubtless overconservative for the kind of joints we are investigating now. On the other hand we have seen (see A.38, A.42) that both the peak current and the power dissipated scale with higher powers of the joint length L itself. We want to prove that a reasonable trade off between steady state dissipation and peak dissipation may be reached if the joint is between 2 and 3 m long. We report the peak current, peak power dissipation, steady state power dissipation, highest temperature rise during transient and steady state conditions in Table 2 and Table 3, for joint lengths from 1 to 5 m. All these quantities are calculated both during the magnet charge with constant ramp rate and during the discharge on 2 mΩ dump resistor.

TAB. 2: Peak current, Peak, Steady and Foucault power dissipation during the magnet ramp-up at dI/dt = 2.85 A/s, along with the induced temperature rise under different hypotheses. †) cooling in the joint zone: Y = yes; N = no; n/a = not applicable. ‡) heat release: P = point-like; D = distributed.

Length [m]	**Peak Current [A]**	**Peak Power [W]**	**Steady Power [W]**	**Foucault Power [W]**	**DT Peak [K]**	**DT Steady [K]**	**DT Peak [K]**	**DT Steady [K]**
					n/a †)	Y†)	N†)	N†)
					P‡)	D‡)	D‡)	D‡)
1.0	20,500	0.173	0.165	0.008	0.027	0.015	0.044	0.042
2.0	21,409	0.150	0.083	0.067	0.024	0.005	0.053	0.029
2.5	25,019	0.205	0.066	0.139	0.032	0.003	0.082	0.027
3.0	30,402	0.304	0.055	0.249	0.048	0.002	0.137	0.025
4.0	43,389	0.591	0.041	0.550	0.093	0.001	0.325	0.023
5.0	55,298	0.872	0.033	0.839	0.137	0.001	0.565	0.021

TAB. 3: Peak current, Peak, Steady and Foucault power dissipation during a dump discharge, along with the induced temperature rise under different hypotheses. †) cooling in the joint zone: Y = yes; N = no; n/a = not applicable. ‡) heat release: P = point-like; D = distributed.

Length [m]	**Peak Current [A]**	**Peak Power [W]**	**Steady Power [W]**	**Foucault Power [W]**	**DT Peak [K]**	**DT Steady [K]**	**DT Peak [K]**	**DT Steady [K]**
					n/a †)	Y†)	N†)	N†)
					P‡)	D‡)	D‡)	D‡)
1.0	20,500	0.167	0.165	0.002	0.026	0.015	0.043	0.042
2.0	22,425	0.222	0.083	0.139	0.035	0.005	0.078	0.029
3.0	31,382	0.367	0.055	0.312	0.058	0.002	0.166	0.025
4.0	40,462	0.474	0.041	0.433	0.074	0.001	0.261	0.023
5.0	48,241	0.532	0.033	0.499	0.083	0.001	0.345	0.021

The Peak Current and Peak Power release are numerical results. The steady state dissipation (Steady Power) was found simply from $R \cdot I_{op}^2$, and the contribution from eddy currents (Foucault Power) is simply the algebraic difference of the two previous quantities. The temperature rise under steady conditions was computed assuming a distributed heat release –as appropriate in this case- with and without cooling in the joint zone. During transient conditions the temperature rise was calculated as follows: first we note that the typical time scale of the current change (say 1000 s) is much larger than the thermal diffusivity (which is in the order of a few seconds); as a consequence we are at any time close to the stationary condition relevant to the dissipation present at that moment (quasi-steady state conditions). We are therefore allowed to exploit the results we found for the steady conditions case described in [1], assuming the relevant power dissipated. The second important point is that the power dissipation does not take place uniformly along the joint, but it is concentrated near the centre, therefore we exploit the solution (Ref [1], Eq. (4)) found for the point-like power release, which represents a more conservative hypothesis with respect to the case of uniformly distributed power release and cooled joint. The hypothesis of no cooling in the joint zone and uniformly distributed power release is considered also. The dump discharge case is not worse than the magnet charge with constant ramp rate, despite the fact that the dI/dt is much higher at the beginning. The reasons for this were explained in the previous section.

6 CONCLUSIONS

We have shown that large eddy currents appear inside a joint when the magnet current is changing. We have investigated in detail both the magnet ramp up and the dump discharge scenarios. If a joint length of 5 m is retained these currents are potentially dangerous since they could exceed the critical value and they increase vastly the power dissipation. Nonetheless from our calculations we find that with a shorter joint length, likely in the range 2 - 3 m, we can achieve a good trade-off between dissipation due to eddy currents and steady state dissipation, both during the magnet charge and dump discharge, thus allowing a safe magnet operation under those conditions.

7 REFERENCES

(1) E.Acerbi, G.Ambrosio, M.Sorbi, G.Volpini, INFN/TC-97/07, 25 febbraio 1997.
(2) G.Volpini, E.Acerbi, G.Ambrosio and M.Sorbi, IEEE Trans on Mag, **9**, no. 2 (1999) pages 193-196.
(3) G. Volpini, M. Pojer, INFN/TC, to be published.
(4) Stanley J. Farlow, "Partial Differential Equations for Scientists and Engineers", (Dover Publications, Inc., New York 1993).

APPENDIX: RESOLUTION OF THE DIFFERENTIAL EQUATION DESCRIBING THE CURRENT INSIDE THE JOINTS

Here we solve analytically the two problems expressed by (5,6) (case a) and (9,6) (case b), assuming constant coefficients. From a mathematical point of view these two problems are expressed by homogeneous (case a), non homogeneous (case b) partial derivatives parabolic differential equations with nonhomogeneous boundary conditions. This kind of problem may be solved with standard techniques described in any textbook on the subject. We have used [4]. Hereafter we report the two problems:

A.1 General method

Case a) - test joint

$$\frac{d}{dt}J(x,t) - \frac{\rho}{2\cdot(\lambda-\mu)}\cdot\frac{d^2}{dx^2}J(x,t) = 0 \qquad (5)$$

$$J(0,t) = I(t)$$

$$J(L,t) = 0 \qquad (6)$$

Case b) - joint inside a coil

$$\frac{d}{dt}J(x,t) - \frac{\rho}{2\cdot(\lambda-\mu)}\cdot\frac{d^2}{dx^2}J(x,t) = \beta\cdot\frac{d}{dt}I(t) \qquad (9)$$

$$J(0,t) = I(t)$$

$$J(L,t) = 0 \qquad (6)$$

where:

$$\beta = \frac{1}{2}\cdot\left(1 - \frac{D\cdot k}{\lambda-\mu}\right) \qquad J(x,t) = \int_x^L j(u)\,du \qquad (A.1)$$

In order to solve these problems, we first switch to a homogeneous boundary conditions system with a suitable change of variable:

$$Y(x,t) = J(x,t) - I(t)\cdot\left(1 - \frac{x}{L}\right) \quad \text{and} \quad u = \frac{x}{L}\,. \qquad (A.2)$$

Eq. (5,6) (case a) become:

$$\frac{d}{dt}Y_a - \alpha^2 \cdot \frac{d^2}{du^2}Y_a = s_a(u,t) \tag{A.3}$$

$$Y_a(0,t) = 0 \tag{A.4}$$

$$Y_a(1,t) = 0$$

where we have used the following positions:

$$\alpha := \sqrt{\frac{\rho}{2\cdot\lambda\cdot L^2}}; \qquad s_a(u,t) = (u-1)\cdot\left(\frac{d}{dt}I(t)\right). \tag{A.5}$$

Similarly (9,6) (case b) now look as follows:

$$\frac{d}{dt}Y_b - \alpha^2 \cdot \frac{d^2}{du^2}Y_b = s_b(u,t) \tag{A.6}$$

$$Y_b(0,t) = 0 \tag{A.7}$$

$$Y_b(1,t) = 0$$

with the position:

$$s_b(u,t) = (u-1+\beta)\cdot\left(\frac{d}{dt}I(t)\right) \quad . \tag{A.8}$$

Where subscripts a and b have been used to remember that the two terms are note the same. With this choice of variables the two problems have homogeneous boundary conditions but are not homogenous themselves. These can be solved by means of the eigenfunction expansion method (Ref. [4], page 64). For both cases the associated homogeneous problem is:

$$\frac{d}{dt}V - \alpha^2 \cdot \frac{d^2}{dx^2}V = 0 \tag{A.9}$$

$$V(0,t) = 0 \tag{A.10}$$

$$V(1,t) = 0$$

whose solution is:

$$V(u,t) = \sum_{n=1}^{\infty} a_n \cdot e^{-(n\cdot\pi\cdot\alpha)^2\cdot t} \cdot \sin(n\cdot\pi\cdot u) \quad . \tag{A.11}$$

According the expansion method, we look for a solution in the form:

$$Y(u,t) = \sum_{n=1}^{\infty} Y(t)_n \cdot \sin(n\cdot\pi\cdot u) \tag{A.12}$$

and we expand s(u,t) on the basis formed by the eigenfunctions of the associated homogeneous equation:

$$s = \sum_{n=1}^{\infty} s_n \cdot \sin(n\cdot\pi\cdot u) \tag{A.13}$$

The precise form of s(u,t) depends on the details of the situation being investigated. Once that the detailed form for the s_n has been found, the explicit form for the $Y_n(t)$ is given by:

$$Y(t)_n = a_n \cdot e^{-(n\cdot\pi\cdot\alpha)^2\cdot t} + \int_0^t e^{-(n\cdot\pi\cdot\alpha)^2\cdot(t-\tau)} \cdot s_n(\tau)\, d\tau \tag{A.14}$$

where the a_n are to be found by the initial conditions. We can insert this back into (A.12) to get *Y(u,t)* and finally by means of the initial change of variables (A.2) we get the analytical form for the solution. The details of this computation depend on the explicit form for *s(u,t)*, so that we analyse the relevant cases in turn.

A.2 Test joint measurement with trapezoidal current time profile.

Since we are in case a), the source term to be used is given by (A.5a):

$$s(u,t) = (u-1)\cdot\left(\frac{d}{dt} I(t)\right) \tag{A.5a}$$

Keeping into account the explicit expression for *I(t)*, (Fig. 5), we can write:

$$s(u,t) = (u-1)\cdot I_{dot} \qquad t_2 < t < t_3 \quad ; \qquad s(u,t) = -(u-1)\cdot I_{dot} \quad t_4 < t < t_5 \tag{A.15}$$

$$s(u,t) = 0 \qquad \text{any other time.} \tag{A.16}$$

As seen above in (A.13), now we expand *s(u,t)* on the basis formed by the eigenfunctions of the associated homogeneous equation:

$$s_n = 2\cdot\int_0^1 s\cdot\sin\left(n\cdot\pi\cdot u\right)\,du \quad . \tag{A.17}$$

When *s(u,t)* is zero (A.16) all the a_n's are zero. For case (A.15a) we have:

$$s_n = 2\cdot I_{dot}\cdot\int_0^1 \sin\left(n\cdot\pi\cdot u\right)\cdot(u-1)\,du = \frac{-2\cdot I_{dot}}{n\cdot\pi} \tag{A.18}$$

Case (A.15b) is analogous, the only difference being the sign. We can summarise these results as follows:

$$s_n = \frac{-2\cdot I_{dot}}{n\cdot\pi} \qquad t_2 < t < t_3 \qquad ; \qquad s_n = \frac{2\cdot I_{dot}}{n\cdot\pi} \qquad t_4 < t < t_5 \tag{A.19}$$

$$s_n = 0 \qquad \text{any other time.} \tag{A.20}$$

We now insert these expressions for s_n back into (A.14), making the further assumption that no current is flowing anywhere in the joint at $t = 0$; the initial condition is therefore zero everywhere, and all the a_n's are zero.

$$Y(t)_n = \int_0^t e^{-(n\cdot\pi\cdot\alpha)^2\cdot(t-\tau)}\cdot s_n(\tau)\,d\tau \quad . \tag{A.21}$$

Now we evaluate explicitly this integral, exploiting (A.15, A.16) for $s_n(t)$'s.

$$Y(t)_n = 0 \qquad t < t_2 \qquad \text{Zero current} \tag{A.22}$$

Increasing ramp:

$$Y(t)_n = \frac{-2\cdot I_{dot}}{n\cdot\pi}\cdot\int_{t_2}^{t} e^{-(n\cdot\pi\cdot\alpha)^2\cdot(t-\tau)}\,d\tau = \frac{-2\cdot I_{dot}\cdot\alpha}{(n\cdot\pi\cdot\alpha)^3}\cdot\left[1 - e^{-(n\cdot\pi\cdot\alpha)^2\cdot(t-t_2)}\right] \qquad t_2 < t < t_3 \tag{A.23}$$

Plateau at full current; here we split the integral in two parts:

$$\begin{aligned} Y(t)_n = \int_0^t e^{-(n\cdot\pi\cdot\alpha)^2\cdot(t-\tau)}\cdot s_n(\tau)\,d\tau = &\int_{t_2}^{t_3} e^{-(n\cdot\pi\cdot\alpha)^2\cdot(t-\tau)}\cdot s_n(\tau)\,d\tau \ \ldots \\ &+ \int_{t_3}^{t} e^{-(n\cdot\pi\cdot\alpha)^2\cdot(t-\tau)}\cdot s_n(\tau)\,d\tau \end{aligned} \tag{A.24}$$

Introducing the explicit form for $s_n(t)$ we get:

$$Y(t)_n = e^{-(n\cdot\pi\cdot\alpha)^2\cdot t}\cdot\left[\frac{-2\cdot I_{dot}\cdot\alpha}{(n\cdot\pi\cdot\alpha)^3}\right]\cdot\left[e^{(n\cdot\pi\cdot\alpha)^2\cdot t_3} - e^{(n\cdot\pi\cdot\alpha)^2\cdot t_2}\right] \qquad t_3 < t < t_4 \tag{A.25}$$

The integral is evaluated in a similar way for each part of the current profile. At the end we obtain the following expressions:

$$\begin{aligned} Y_n(t) &= 0 && t < t_2 \\ Y_n(t) &= \frac{-2\cdot I_{dot}\cdot\alpha}{(n\cdot\pi\cdot\alpha)^3}\cdot\left[1 - e^{(n\cdot\pi\cdot\alpha)^2\cdot(t_2-t)}\right] && t_2 < t < t_3 \\ Y_n(t) &= \frac{-2\cdot I_{dot}\cdot\alpha}{(n\cdot\pi\cdot\alpha)^3}\cdot\left[e^{(n\cdot\pi\cdot\alpha)^2\cdot(t_3-t)} - e^{(n\cdot\pi\cdot\alpha)^2\cdot(t_2-t)}\right] && t_3 < t < t_4 \\ Y_n(t) &= \frac{-2\cdot I_{dot}\cdot\alpha}{(n\cdot\pi\cdot\alpha)^3}\cdot\left[e^{(n\cdot\pi\cdot\alpha)^2\cdot(t_3-t)} - e^{(n\cdot\pi\cdot\alpha)^2\cdot(t_2-t)} \ \ldots \right. \\ &\qquad \left. + e^{(n\cdot\pi\cdot\alpha)^2\cdot(t_4-t)} - 1\right] && t_4 < t < t_5 \\ Y_n(t) &= \frac{-2\cdot I_{dot}\cdot\alpha}{(n\cdot\pi\cdot\alpha)^3}\cdot\left[e^{(n\cdot\pi\cdot\alpha)^2\cdot(t_3-t)} - e^{(n\cdot\pi\cdot\alpha)^2\cdot(t_2-t)} \ \ldots \right. \\ &\qquad \left. + e^{(n\cdot\pi\cdot\alpha)^2\cdot(t_4-t)} - e^{(n\cdot\pi\cdot\alpha)^2\cdot(t_5-t)}\right] && t > t_5 \end{aligned} \tag{A.26}$$

If we define the following function; $MN0(x,y) := \Phi(y-x)\cdot(x-y)$, where *F(x)* is the Heaviside step function, all the above expressions merge in one:

$$Y_n(t) = \frac{-2\cdot I_{dot}\cdot\alpha}{(n\cdot\pi\cdot\alpha)^3}\cdot\left[\begin{array}{l} e^{(n\cdot\pi\cdot\alpha)^2\cdot MN0(t_3,t)} - e^{(n\cdot\pi\cdot\alpha)^2\cdot MN0(t_2,t)} \ldots \\ + e^{(n\cdot\pi\cdot\alpha)^2\cdot MN0(t_4,t)} - e^{(n\cdot\pi\cdot\alpha)^2\cdot MN0(t_5,t)} \end{array}\right] . \qquad (A.27)$$

Now, from the expression seen above for *J(x,t)* (A.2), and the expansion for *Y(x,t)*, (A.12), we can write the explicit expression for the integrated current density:

$$J(x,t) = I(t)\cdot\left(1-\frac{x}{L}\right) + \sum_{n=1}^{\infty} Y_n(t)\cdot\sin\left(n\cdot\pi\cdot\frac{x}{L}\right) \quad . \qquad (A.28)$$

The current density may be found differentiating (A.28) with respect to *x*.

$$j(x,t) = -\frac{d}{dx}\cdot J(x,t) = \frac{1}{L}\cdot\left(I(t) - \pi\cdot\sum_{n=1}^{\infty} Y_n(t)\cdot n\cdot\cos(n\cdot\pi\cdot u)\right) \quad . \qquad (A.29)$$

A.3 Magnet joint behaviour during charge or discharge with constant ramp rate.
Here we are in case b) and the source term *s* has the following form:

$$s_b(u,t) = (u-1+\beta)\cdot\left(\frac{d}{dt}I(t)\right) \qquad (A.8)$$

We consider a ramp at constant rate, followed by a plateau at constant current, so that *I(t)* is:

$$\begin{array}{ll} s(u,t) = 0 & t < t_0 \\ s(u,t) = (u-1+\beta)\cdot I_{dot} & t_0 < t < t_1 \\ s(u,t) = 0 & t > t_1 \end{array} \qquad (A.30)$$

As seen above (A.13), now we expand *s(u,t)* on the basis formed by the eigenfunctions of the associated homogeneous equation:

$$\begin{aligned} s_n &= 0 && t < t_0 \\ s_n &= 2\cdot I_{dot}\cdot\int_0^1 \sin(n\cdot\pi\cdot u)\cdot(u-1+\beta)\,du = \frac{2\cdot I_{dot}}{n\cdot\pi}\cdot\left[\beta\cdot\left[1-(-1)^n\right]-1\right] && t_0 < t < t_1 \\ s_n &= 0 && t > t_1 \end{aligned} \tag{A.31}$$

We now come back to (A.14); in this case the initial condition is 0 everywhere both for charge and for discharge since *Y(x,t)* is the "homogeneous boundary" solution. As a consequence, all the a_n*'s* are zero, and the expression for $Y_n(t)$ is the same as (A.21) with the proper $s_n(t)$. The integration is straightforward and gives:

$$\begin{aligned} Y_n(t) &= 0 && t < t_0 \\ Y_n(t) &= \frac{2\cdot I_{dot}\cdot\alpha}{(n\cdot\pi\cdot\alpha)^3}\cdot\left[\beta\cdot\left[1-(-1)^n\right]-1\right]\cdot\left[1-e^{(n\cdot\pi\cdot\alpha)^2\cdot(t_0-t)}\right] && t_0 < t < t_1 \\ Y_n(t) &= \frac{2\cdot I_{dot}\cdot\alpha}{(n\cdot\pi\cdot\alpha)^3}\cdot\left[\beta\cdot\left[1-(-1)^n\right]-1\right]\cdot\left[e^{(n\cdot\pi\cdot\alpha)^2\cdot(t_1-t)}-e^{(n\cdot\pi\cdot\alpha)^2\cdot(t_0-t)}\right] && t > t_1 \end{aligned} \tag{A.32}$$

Or, with the same *MN0* function introduced above,

$$Y_n(t) = \frac{2\cdot I_{dot}\cdot\alpha}{(n\cdot\pi\cdot\alpha)^3}\cdot\left[\beta\cdot\left[1-(-1)^n\right]-1\right]\cdot\left[e^{(n\cdot\pi\cdot\alpha)^2\cdot MN0(t_1,t)}-e^{(n\cdot\pi\cdot\alpha)^2\cdot MN0(t_0,t)}\right] \tag{A.33}$$

from which we get the explicit expressions for the integrated current density (see (A.2) and (A.12)):

$$J(x,t) = I(t)\cdot\left(1-\frac{x}{L}\right)+\sum_{n=1}^{\infty} Y_n(t)\cdot\sin\left(n\cdot\pi\cdot\frac{x}{L}\right) \tag{A.34}$$

Which, differentiated with respect to x, gives the current density:

$$j(x,t) = -\frac{d}{dx}\cdot J(x,t) = \frac{1}{L}\cdot\left(I(t)-\pi\cdot\sum_{n=1}^{\infty} Y_n(t)\cdot n\cdot\cos(n\cdot\pi\cdot u)\right) \quad . \tag{A.35}$$

These expressions are formally identical to (A.28) and (A.29), although the appropriate forms for $Y_n(t)$ and $I(t)$ must be taken in both cases.

A.4 Peak current estimate.

The peak current is reached at the end of the current ramp-up, at about one half of the joint length, as it can be seen in the above figures. Its value is therefore found from (A.34), estimated at $x = L/2, \quad t = t_1$:

$$J_{peak} = J\left(\frac{L}{2}, t_1\right) = \frac{I_{max}}{2} + \sum_{n=1}^{\infty} Y_n(t_1)\cdot\sin\left(\frac{n}{2}\cdot\pi\right) = \frac{I_{max}}{2} + \sum_{n=0}^{\infty} Y_{2\,n+1}(t_1)\cdot(-1)^n \,, \tag{A.36}$$

which, after some manipulations becomes:

$$J_{peak} = \frac{I_{max}}{2} - \frac{2\cdot I_{dot}\cdot D\cdot k}{\alpha^2\cdot\pi^3\cdot\lambda}\cdot\sum_{n=0}^{\infty}\frac{(-1)^n}{(2\cdot n+1)^3}\cdot\left[1 - e^{[(2\cdot n+1)\cdot\pi\cdot\alpha]^2\cdot(t_0 - t_1)}\right] \quad . \tag{A.37}$$

The sum has alternating signs, so that the maximum error is equal to the modulus of the first neglected term; in practice the contribution from the second term (included) on is less than 2%, if the ramp up time is not much smaller than the time constant $(\pi\cdot\alpha)^{-2}$. In this approximation we can write:

$$J_{peak} = \frac{I_{max}}{2} - \frac{4\cdot I_{dot}\cdot D\cdot k\cdot L^2}{\rho\cdot\pi^3}\cdot\left[1 - e^{(\pi\cdot\alpha)^2\cdot(t_0 - t_1)}\right] \tag{A.38}$$

A.5: The power dissipated inside a joint during the magnet ramp.

The total power dissipated along the junction (Sec. 5.1.4) is given by:

$$\rho\cdot\int_0^L j(s)^2\,ds \tag{A.39}$$

Introducing the explicit form for $j(x)$, (A.35), we get:

$$\frac{\rho}{L}\cdot\int_0^1\left(I(t)-\pi\cdot\sum_{n=1}^{\infty}Y(n,t)\cdot n\cdot\cos\left(n\cdot\pi\cdot s\right)\right)^2 ds \qquad (A.40)$$

$$\frac{\rho}{L}\cdot\left[I(t)^2+\pi^2\cdot\int_0^1\left(\sum_{n=1}^{\infty}Y(n,t)\cdot n\cdot\cos\left(n\cdot\pi\cdot s\right)\right)^2 ds-2\cdot\pi\cdot I(t)\cdot\sum_{n=1}^{\infty}Y(n,t)\cdot n\cdot\int_0^1\cos\left(n\cdot\pi\cdot s\right)ds\right]$$

Since $\int_0^1\cos\left(n\cdot\pi\cdot s\right)ds=0$ for all *n*, the rightmost term is zero.

$$\frac{\rho}{L}\cdot\left[I(t)^2+\pi^2\cdot\int_0^1\left(\sum_{n=1}^{\infty}\sum_{m=1}^{\infty}Y(n,t)\cdot Y(m,t)\cdot n\cdot m\cdot\cos\left(n\cdot\pi\cdot s\right)\cdot\cos\left(m\cdot\pi\cdot s\right)\right)ds\right]$$

Here we exchange sums and integrals, so that:

$$\frac{\rho}{L}\cdot\left(I(t)^2+\pi^2\cdot\sum_{n=1}^{\infty}\sum_{m=1}^{\infty}Y(n,t)\cdot Y(m,t)\cdot n\cdot m\cdot\int_0^1\cos\left(m\cdot\pi\cdot s\right)\cdot\cos\left(n\cdot\pi\cdot s\right)ds\right)$$

$$\frac{\rho}{L}\cdot\left(I(t)^2+\frac{\pi^2}{2}\cdot\sum_{n=1}^{\infty}\sum_{m=1}^{\infty}Y(n,t)\cdot Y(m,t)\cdot n\cdot m\cdot\delta_{nm}\right)$$

The final expression for the total power dissipated in a joint is therefore:

$$Q(t)=\frac{\rho}{L}\cdot\left(I(t)^2+\frac{\pi^2}{2}\cdot\sum_{n=1}^{\infty}Y(n,t)^2\cdot n^2\right). \qquad (A.41)$$

The behaviour of the first term ('Joule' term) is clear: the power scales as r and as L^{-1} . The ramp rate I_{dot} has obviously no effect. To understand better the 'Foucault' term, let us come back to the expression for the functions (A.29):

$$Y_n(t) = \frac{2 \cdot I_{dot}}{\alpha^2} \cdot y_n(t)$$

where

$$y_n(t) = \frac{\beta \cdot \left[1 - (-1)^n\right] - 1}{(n \cdot \pi)^3} \cdot \left[e^{(n \cdot \pi \cdot \alpha)^2 \cdot MN0(t_1, t)} - e^{(n \cdot \pi \cdot \alpha)^2 \cdot MN0(t_0, t)} \right]$$

$$\frac{8 \cdot \pi^2 \cdot I_{dot}{}^2 \cdot \lambda^2 \cdot L^3}{\rho} \cdot \sum_{n=1}^{\infty} y(n,t)^2 \cdot n^2 \qquad \text{(A.42)}$$

A.6 Exponential current decrease

A third possible situation is represented by the exponential current decrease with time constant t. In this case the source term (A.5) is:

$$s_c(u,t) = (u - 1 + \beta) \cdot \frac{d}{dt} I(t)$$

Introducing the form for *I(t);*

$$I(t) = I(t_0) \cdot e^{\frac{t_0 - t}{\tau}} \qquad \text{(A.43)}$$

We get:

$$s_c(u,t) = 0 \qquad t < t_0$$

$$s_c(u,t) = -(u - 1 + \beta) \cdot \frac{I(t_0)}{\tau} \cdot e^{\frac{t_0 - t}{\tau}} = \frac{-1}{\tau} \cdot (u - 1 + \beta) \cdot I(t) \qquad t \geq t_0$$

The expansion of $s_n(u,t)$ on the s basis is:

$$\begin{aligned} s_n &= 0 && t < t_0 \\ s_n &= 2\cdot\int_0^1 s\cdot\sin\left(n\cdot\pi\cdot u\right)du = \frac{-2\cdot I(t)}{\tau}\cdot\frac{\left[\beta\cdot\left[1-(-1)^n\right]-1\right]}{n\cdot\pi} && t \geq t_0 \end{aligned} \quad . \qquad \text{(A.44)}$$

The $Y_n(t)$ are given by (A.16) (the same comments apply here):

$$Y(t)_n = \int_0^t e^{-(n\cdot\pi\cdot\alpha)^2\cdot(t-\vartheta)}\cdot s_n(\vartheta)\,d\vartheta$$

Now we evaluate explicitly this integral, exploiting (A.44) for $s_n(t)'s$.

$$Y(t)_n = 0 \qquad t < t_0$$

$$Y(t)_n = \frac{-2\cdot I(t_0)}{\tau}\cdot\frac{\left[\beta\cdot\left[1-(-1)^n\right]-1\right]}{n\cdot\pi}\cdot\int_{t_0}^t e^{-(n\cdot\pi\cdot\alpha)^2\cdot(t-\vartheta)+\frac{t_0-\vartheta}{\tau}}\,d\vartheta \qquad t \geq t_0$$

and after the integration we find:

$$Y(t)_n = -2\cdot I(t_0)\cdot\frac{\beta\cdot\left[1-(-1)^n\right]-1}{n\cdot\pi\cdot\left[(n\cdot\pi\cdot\alpha)^2\cdot\tau-1\right]}\cdot\left[e^{\frac{-(t-t_0)}{\tau}} - e^{\left[-(n\cdot\pi\cdot\alpha)^2\cdot(t-t_0)\right]}\right] \qquad t \geq t_0$$

As usual we write:

$$Y(t)_n = -2\cdot I(t_0)\cdot\frac{\beta\cdot\left[1-(-1)^n\right]-1}{n\cdot\pi\cdot\left[(n\cdot\pi\cdot\alpha)^2\cdot\tau-1\right]}\cdot\left[e^{\frac{MN0(t_0,t)}{\tau}} - e^{\left[(n\cdot\pi\cdot\alpha)^2\cdot MN0(t_0,t)\right]}\right] \qquad \text{(A.45)}$$

Valid at any time. For the overall current flowing into the Rutherford we can -as already seen- take (A.28) and (A.29), provided that the appropriate expressions for $Y_n(t)$ and $I(t)$ are used, (A.45) and (A.44) respectively.